Upstream Oil and Gas Technology, Volume 7, September 2021, Article number 100037
DOI: 10.1016/j.upstre.2021.100037

CFD study of the characteristics of a single elongated gas bubble in liquid in a moderately inclined pipe

Aniefiok Livinus[1], Patrick G. Verdin[2]

1. Chemical and Petroleum Engineering Department, University of Uyo, P.M.B 1017, Uyo, Akwa Ibom State, Nigeria.
2. Energy & Power, School of Water, Energy and Environment, Cranfield University, MK43 0AL, UK.

ABSTRACT

In recent years, Computational Fluid Dynamics (CFD) modelling methods have been applied to study the behavior of a single elongated bubble in stagnant and flowing liquid. To date, only very few studies have been performed for slightly upwardly inclined pipes. This work presents mostly 2D numerical simulations based on the Volume of Fluid approach, dealing with the characteristics of a single elongated bubble injected into a liquid in a slightly upwardly inclined pipe. CFD-based results were compared with experimental results. In general, except the numerical bubble length, drift velocity, bubble fraction and bubble shape, agreed fairly with the experimental outcomes.

Keywords: CFD; large gas bubble characteristics; bubble length; upward flow.

Nomenclature

C_o	Constant (in translational velocity)	
D	Pipe diameter	m
Eo	Eötvös Number	
Fr	Froude Number	
g	Acceleration due to gravity	m/s^2
Mo	Morton number	
Re	Reynolds number	
N_f	Viscosity number	
v_d	Drift velocity	m/s
v_m, U_m	Mixture velocity	m/s
v_t, V_{TB}	Translational velocity	m/s
V_{so}	Superficial velocity of oil	m/s
ρ	Density	kg/m^3
μ	Viscosity	$kgm^{-1}s^{-1}$
σ	Surface tension	N/m
θ	Pipe inclination to horizontal	Degree
L	Pipe length	m
L_b	Bubble length determined from experiment	m

$Sim.L_b$	Bubble length determined from simulations	m
VOLgas	Estimated gas volume injected during experiment	m^3

1. INTRODUCTION

When gas and liquid flow in a pipe with varying flow rates, they tend to form a variety of flow regimes; one of such flow patterns is the slug flow. This kind of flow can be frequently found in the production and transportation of oil as it occurs over a wide range of intermediate flow rates of gas and liquid. It can create pressure fluctuations, which can have adverse effects on the oil and gas transport and facilities. Slug flow is also of interest for many industrial processes, for instance boiling and condensation processes in power generation facilities, chemical plants and refineries.

The intermittent slug flow phenomena have been systematically investigated over the years in well-controlled experiments, especially adopting the approach of the propagation of a single elongated bubble in stagnant or flowing liquid in pipes, as in the works of Bendiksen [1], Weber et al. [2], Hasan and Kabir [3], Viana et al. [4], Gokcal et al. [5], Jeyachandra et al. [6], Moreiras et al. [7], Losi and Poesio [8], Livinus et al. [9]. The overall objective of these studies has been to acquire data for improving the modelling of slug flow phenomena. Most of the experimental works have provided information on the effects of pipe inclination and pipe size on the bubble velocity, void fractions, and the forms of the liquid film – stratified or annular. Unfortunately, only very few experiments have been reported on the characteristics of the bubble length. In addition, the bubble length measurements have been reported only for a point along the pipe.

In recent years, Computational Fluid Dynamics (CFD) modelling methods have been applied to study the intermittent slug flow phenomena. Cook and Behnia, [10], Taha and Cui [11], Ujang et al. [12], Hua et al. [13] investigated such kind of flow by modelling the behaviour of a single elongated bubble in stagnant and flowing liquid. A detailed literature review of some of the previous studies based on the CFD modelling of an elongated bubble in liquid in pipes is presented in Table 1. It can be seen that several researchers have been able to model the motion of large bubbles in liquid in vertical, horizontal and inclined pipes by adopting different methods to reduce the requirements of their computational resources, such as the use of a 2D vertical axisymmetric approach for the Taylor bubble case, 3D structured grids with symmetric boundary conditions, the assumption of a particular volume of bubble to be already present in the domain, the strategic mesh refinement of the pipe geometry model, and the reduction of the pipe length. Different methods were also applied to track the interface of the gas and liquid phases and to calculate the fluid fluxes across the control volume faces such as the use the Volume of Fluid (VOF) method from Hirt and Nichols [14], the geometric reconstruction scheme based on the piece linear interface calculation (PLIC) method of Youngs [15], and the Level Set method of Osher and Sethian [16]. A moving reference frame was also used by several researchers, e.g. Hua et al. [13], to follow the movement of an elongated bubble.

To date, most CFD studies have targeted the bubble velocity and bubble fraction, and results tend to agree with experimental measurements. It is important to note that CFD results for high viscous fluid

have shown that the drift velocity of the gas bubble in a horizontal pipe not only decreases with decreasing Reynolds number, but also decreases as it travels along the pipeline, as reported in Andreussi et al. [17], Ramdin and Henkes [18]. The CFD studies of elongated bubbles described in the above literature were mostly performed when assuming that a particular volume of bubble was already present in the domain. The modelling approaches employed by these authors were not used to investigate the bubble length but only the bubble rise velocity profile and the bubble shape. Thus, the CFD described here looks at the bubble development in a pipe, under similar conditions as those reported in the experimental works of Livinus and Verdin [25], and Livinus [26]. The pipe geometry represents the full length of the test pipe. The mesh is strategically refined in different regions, mostly next to the walls to improve the simulation results. This paper discusses mostly 2D VOF-based numerical simulations on the characteristics of a single elongated gas bubble injected into a liquid in a slightly upwardly inclined pipe. The CFD-based results including bubble velocity, void fractions, and bubble length are compared with experimental results, when available.

Table 1: Summary of CFD studies of large bubbles in liquid in pipes

Sources	Pipe and fluid properties	CFD approach	Investigations
Cook and Behnia [10] (2001)	ρ = 998.2, 1113kg/m^3; μ = 0.001, 0.021kg/m^{-1}s^{-1}; σ = 0.0736, 0.048N/m; D = 0.032, 0.0445, 0.05, 0.178-m; θ = 5-75^o; L = 1m.	3D symmetric boundary, VOF technique using ANSYS FLUENT®. Placed an initial gas volume in the liquid filled pipe.	Effect of surface tension, pipe diameter and tube inclination on bubble velocity.
Taha and Cui [11] (2006)	ρ = 1129-1223kg/m^3; Eo = 0.062-0.066; N_f = 176-1528; D =0.019m; θ = 90^o; L =11D	2D axisymmetric and 3D simulations with VOF method using ANSYS FLUENT®.	Shape and velocity distributions, local wall shear stress distribution.
Andreussi et al [17] (2009)	μ = 0.001, 0.121, 0.692-kg/m^{-1}s^{-1}; D = 0.0508m; θ = 0^o; L = 3m;	3D simulations with VOF method using ANSYS FLUENT®. 1-D transient flow simulations using MAST®.	Bubble velocity, dimensionless liquid height.
Ben-Mansour et al. [19] (2010)	ρ = 880kg/m^3; μ = 0.001, 0.015, 0.120, 0.250, 0.600, 1.2-kg/m^{-1}s^{-1}; σ = 0.03N/m; D = 0.0508, 0.0762, 0.1524-m; θ = 0^o.	2D and 3D simulations with VOF technique using ANSYS FLUENT®.	Bubble velocity and dimensionless liquid height.
Ramdin and Henkes [18] (2012)	Inviscid fluid with and without surface tension, Re = 6, 26, 45, 253, where $Re = \frac{\rho L_x \sqrt{g L_x}}{\mu}$, L_x is characteristic length,	2D and 3D simulations with VOF technique using ANSYS FLUENT®.	Bubble velocity expressed in terms of Froude number.

	for 2D, L_x = channel height, H, for 3D L_x = D; θ = 0° and 90°.		
Hua et al. [13] (2012)	ρ = 998kg/m^3; μ = 0.001kg/m^{-1}s^{-1}; D = 0.1m; L = 20D; θ = 0°:5°:90°.	3D simulations with VOF technique using ANSYS FLUENT®.	Bubble propagating hydrodynamics in both flowing and stagnant liquid, turbulence models performance.
Liné et al. [20] (2013)	ρ_l = 883kg/m^3, ρ_g = 20.5kg/m^3; μ = 0.014kg/m^{-1}s^{-1}; D = 0.1524m; L = 100D; θ = 0°.	3D simulations with Level set formulation using ANANAS^{TM} software code.	Slug flow simulation, and validated in terms of Taylor bubble velocity, bubble fraction, gas and liquid superficial velocity in a unit cell.
Kroes and Henkes [21] (2014)	Inviscid fluid, Re = 1, 3, 10, 30, 100, 300, 1000, 3000, 10000. where $Re = \frac{\rho L_x \sqrt{g L_x}}{\mu}$, L_x is characteristic length, for 2-D, L_x = channel height, H, for 3D L_x = D; θ = 0°	2D and 3D simulations with VOF technique using ANSYS FLUENT®.	Bubble shape and bubble velocity.
Lizarraga-Garcia et al. [22] (2015)	Eo = 76.5, 187, 31.2, 38.6, 98.4, 9.88, 192, 747, 181, 23.8. θ = 5° - 90°	3D simulations with Level set formulation using TransAT® software code.	Motion of Taylor bubbles in slug flow with emphasis on bubble velocity.
Deendarlianto et al. [23] (2016)	ρ_l = 998kg/m^3, ρ_g= 20.5kg/m^3; μ = 0.001kg/m^{-1}s^{-1}; D = 0.026m; L = 1m; θ = 0°.	3D simulations with VOF technique using ANSYS FLUENT®.	Gas-liquid plug flow with emphasis on elongated bubble length and liquid hold up.

2. Simulation methodology

2.1 Pipe geometry

The pipe geometry used for the CFD simulations includes T-shaped junctions at both inlet and outlet, which is similar to one of the experimental test sections. The pipe diameter, D, is 0.099m, and the pipe is 15.7m long. The ratio of the test section length to pipe diameter is about 158. The internal diameter of the gas inlet is 0.004m. 2D and 3D geometries were constructed, and quadrilateral and hexahedral type meshes were generated, see Figure 1. Figure 1(a) shows the full 3D geometry, Figure 1(b) shows a partial view of the 3D mesh, and Figure 1(c) shows a partial view of the 2D planar mesh from the inlet section. The mesh is finer near the wall of the pipe and in the injection area. The mesh is then exported to the flow solver, and a suitable multiphase model is selected. A mesh independence study was performed to ensure the solution is not affected by the mesh resolution.

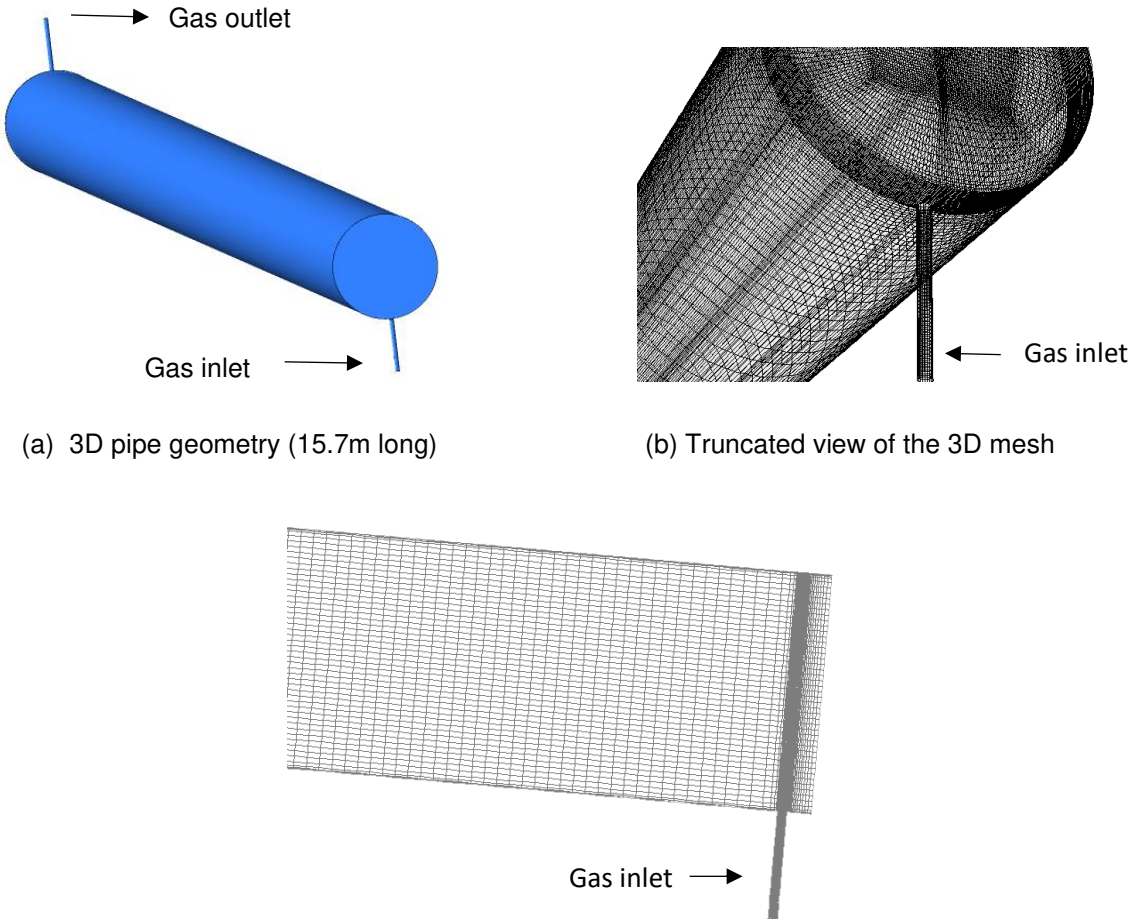

(a) 3D pipe geometry (15.7m long)

(b) Truncated view of the 3D mesh

(c) Truncated view of the 2D planar mesh

Figure 1: Pipe geometry model

2.2 VOF multiphase model

The volume of fluid (VOF) model implemented in ANSYS FLUENT was applied to capture phase distributions. As mentioned previously, the VOF model is based on the work of Hirt and Nichols [14]. It is a surface tracking method applied on a fixed Eulerian grid which is used to model two or more immiscible fluids where the interface between the fluids is of interest. In the VOF model, a single set of conservation equations is shared by the phases, and the volume fraction for each of the phases is tracked throughout the domain. The interphase between the liquid phase α_l (the primary phase) and the gas phase α_g (the secondary phase) is tracked by solving the conservation equation for the volume fraction of the secondary phase.

$$\frac{\partial(\alpha_g \rho_g)}{\partial t} + \nabla \cdot \left(\alpha_g \rho_g \mathrm{u}\right) = 0 \qquad (1)$$

The volume fraction is solved only for the secondary phase and the volume fraction for the primary phase is obtained using the following constraint.

$$\alpha_l + \alpha_g = 1 \tag{2}$$

The phase volume fraction has a value of 0 or 1 when a control volume is entirely filled with liquid or gas, and a value between 0 and 1 if an interface is present in the control volume.

The VOF model solves a single momentum equation, which is given by:

$$\frac{\partial}{\partial t}(\rho u) + \nabla \cdot (\rho u \cdot u) = -\nabla p + \nabla \cdot [\mu(\nabla u + \nabla u^T)] + \rho g + F \tag{3}$$

The properties that appear in the momentum equations are volume-fraction-averaged properties.

The term *F* in the momentum equation stands for the contribution of surface tension. The continuum surface force (CSF) model proposed by Brackbill et al. [24] was used. It is dependent on the surface tension coefficient, *σ*, and the curvature of the interface, *k*.

$$F = \sigma k \frac{\rho \nabla \alpha_g}{1/2\left(\rho_l - \rho_g\right)} \tag{4}$$

The curvature, *k*, is defined in terms of the divergence of the unit vector normal to the wall, $\hat{n}$.

$$k = \nabla \cdot \hat{n} \tag{5}$$

$$\hat{n} = \frac{n}{|n|} \tag{6}$$

where n is the surface normal, expressed as the gradient of the volume fraction of the gas phase, α_g.

$$n = \nabla \alpha_g \tag{7}$$

The Brackbill et al. [24] approach is used to model the effect of wall adhesion at fluids interfaces in contact with rigid boundaries. The unit surface normal at the live cell next to the wall is replaced by the following equation, which is the so-called dynamic boundary condition, resulting in adjustment of the curvature of the surface near the wall:

$$\hat{n} = \hat{n}_l \cos\theta_l + \hat{t}_l \sin\theta_l \tag{8}$$

where $\hat{n}_l$ and $\hat{t}_l$ are the unit vectors normal and tangential to the wall, respectively. The contact angle θ_l is the angle between the wall and the tangent to the interface at the wall.

2.3 Simulation set-up

The initial and boundary conditions, and the numerical solution set-up for all simulations are presented in this section.

2.3.1 Initial and boundary conditions

The initial and boundary conditions for the simulations of the single elongated bubble are similar to the conditions of the experimental matrix of interest. A pressure gas inlet boundary condition for a specific

simulation time is set up at the inlet, and afterwards changed to a wall, to mimic the opening and closing of the injected gas into the system. A constant atmospheric pressure, a gauge pressure of zero, is specified at the outlet. A no-slip boundary condition is imposed at the walls, and gravity is set in the normal downward orientation. The pipe is initially filled with liquid.

2.3.2 Numerical solution set-up

The transient solver is applied in all simulations. Because of the liquid viscosity investigated in this work, the flow is considered to be laminar and thus no turbulence model has been selected in this study. The pressure-based segregated algorithm is applied to solve the transport equations, PRESTO! (pressure staggering option) is used for the pressure interpolation, PISO is set for the pressure-velocity coupling, and either the QUICK or the second-order upwind schemes are applied for the momentum equation. The Geo-Reconstruct scheme is used at the gas-liquid interface. A small time-step of 10^{-5} s is applied first to stabilise the flow and is slowly increased to 10^{-4} s and up to 10^{-3} s. Convergence is judged based on transport equation residuals for which the default criteria are used (10^{-3}) for continuity and momentum equations.

3. Results and Discussions

Three different grid sizes were first considered for the mesh independence study. Two numerical schemes, the second order upwind scheme and the QUICK scheme used for the discretization of the momentum term were also examined. Simulations are based on the experimental flow conditions: 160cP oil viscosity, 870kg/m^3 oil density, 1.75kg/m^3 nitrogen gas density, 0.099m pipe diameter, 3.8-4 bar gas injection pressure, 2 seconds gas injection time. The injection tube has a diameter of 0.004m and the pipe inclination is 5-7.5° from horizontal. These pipe inclinations are chosen as it has been established that the measured results (the void fractions) seems to remain constant after 5°. Table 2 summarizes the experimental data for the preliminary simulation runs.

Table 2: Experimental data for the preliminary simulation runs

Exp. ID	Pipe diam. (m)	Inclination angle (degree)	Inlet pressure (Bar)	Inlet pipe diam. (m)	Injection time (s)	Oil viscosity (cP)	Oil density (Kg/m^3)	Surface tension (N/m)
EXP1	0.099	5	3.8	0.004	1	160	870	0.027
EXP2	0.099	5	3.8	0.004	2	160	870	0.027

To calculate the bubble velocity, the liquid fraction, and the bubble length, iso-surfaces are created. The bubble velocity is calculated by dividing the difference of two/three determined positions of a fully established bubble nose by the corresponding transit simulation fluid flowing time. The bubble length is estimated by determining the distance between the bubble nose and its tail. The preliminary simulation results of the 2D cases for the three different grid sizes and numerical schemes examined are presented

in Table 3. Generally, a low discrepancy (about 3.9%) on the average bubble velocity results is obtained between the coarse mesh of 76,000 cells and the fine mesh of 150,000 cells. The very fine mesh of 610,000 cells gives a bubble velocity result with a deviation of 5.6% from both the coarse mesh and the fine mesh. The bubble length results obtained from the three different grid sizes show an average discrepancy of 1.1%.

Table 3: Mesh independence study for 2D cases

		QUICK Scheme		Second Order Upwind Scheme	
		a		b	
Simulation/Exp. ID	Mesh size (Millions of cells)	Drift velocity (m/s)	Bubble length (m)	Drift velocity (m/s)	Bubble length (m)
2D-EXP1_1	0.076	0.3767	0.8900	0.3558	0.8900
2D-EXP1_2	0.15	0.3697	0.8600	0.3698	0.8900
2D-EXP1_3	0.61	0.3367	0.9000	0.3356	0.8800
2D-EXP2_1	0.076	0.3767	1.9750	0.3721	2.0000
2D-EXP2_2	0.15	0.3790	1.8000	0.3697	1.9900
2D-EXP2_3	0.61	0.3370	1.9000	0.3372	2.0000
EXP1	-	0.432	0.2	-	-
EXP2	-	0.434	0.47	-	-

The simulated bubble velocity obtained from the third order QUICK scheme decreases as the mesh is refined. For the second order upwind scheme however, the simulated velocity increases and then decreases as the mesh is changed from a coarse to a very fine mesh. For a fixed refined mesh, both the QUICK and second order schemes predict almost a similar drift velocity value, which agrees fairly with the experimental results. From the mesh independency and the numerical schemes simulation results, it appears that using a higher order scheme in a very refined mesh for the advection terms in the Navier-Stokes equations does not necessarily lead to more accurate results. The reason for this, as pointed out by Ramdin and Henkes [18], is that for a better accuracy (i.e., more accurate results for a certain number of grid cells), not only the advection terms, but also all other terms in the equations should have been represented by a higher-order scheme.

To maximize computational resources and also achieve distinct interphase of the bubble and the liquid phases, based on the preliminary results, a fine 2D mesh size of 150,000 cells has been chosen for the simulations. Note that this choice is mainly based on the drift velocity as those results were the closest to the experimental results. Despite having a fair drift velocity prediction, the simulated results did not

show a bubble length in agreement with the measurements. This is due to the simplification of the governing equations of the fluid flow in a 2D form. The hydrodynamics of the bubble in stagnant liquid in pipe are significantly affected by the third direction and the surface area of the circular wall. Furthermore, the quantity of gas injected in the system might be higher in the numerical study. As the gas flow rate was not measured at the injection point, the only information available was the pressure of the injected gas and the duration of the gas injection.

3.1 Bubble characteristics

Figure 2 shows the time evolution of a typical elongated bubble formation for a 0.099m diameter, 15.7 m long pipe inclined at 5° from horizontal. The bubble propagates from right to left inside the domain. In most of the simulation runs, a typical elongated bubble shape is formed within 2-3 seconds after injection has stopped. The blue colour represents the gas phase while the red colour represents the oil phase. The front of the bubble is well curved and its shape remains constant as the bubble advances, while the tail changes considerably with time. The degeneration of the tail was inconsequential 6m far from the inlet. Entrainment of dispersed gas in the liquid behind the bubble is observed, which is different for the three mesh sizes and the numerical schemes investigated.

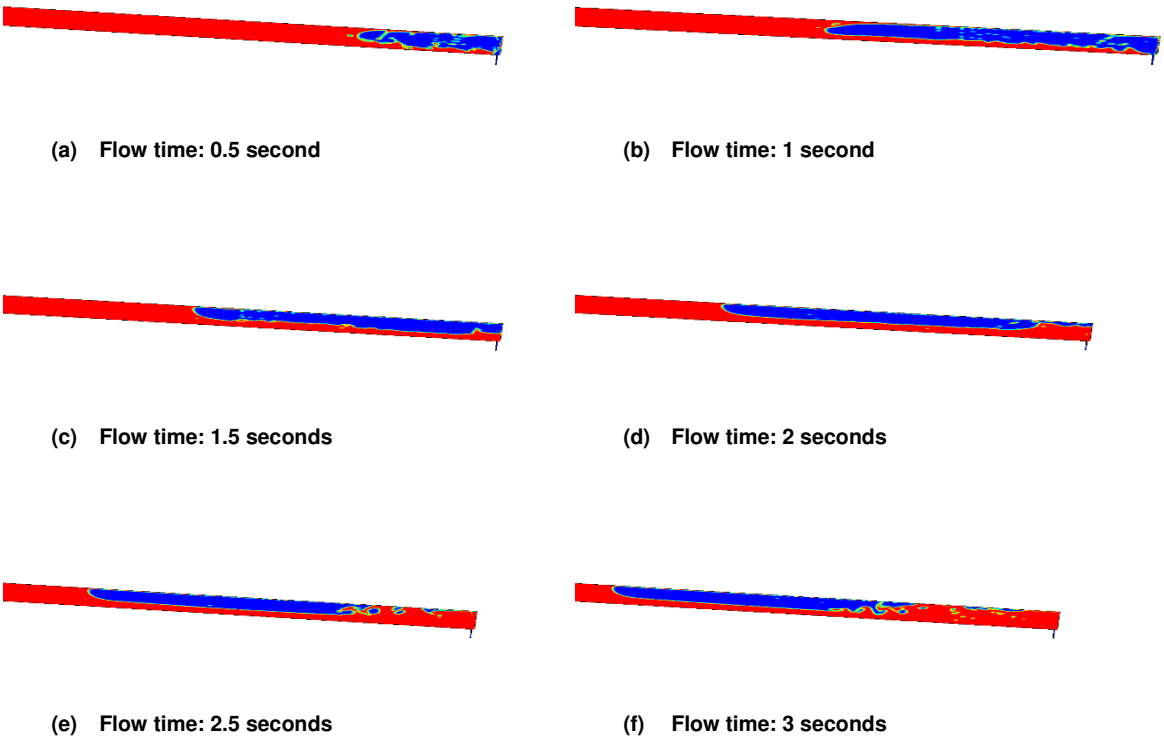

(a) Flow time: 0.5 second **(b) Flow time: 1 second**

(c) Flow time: 1.5 seconds **(d) Flow time: 2 seconds**

(e) Flow time: 2.5 seconds **(f) Flow time: 3 seconds**

Figure 2: Time evolution of a typical elongated bubble formation for EXP2 case

The bubble nose is in good agreement with the experimental data, as can be seen in Figures 3 and 4 for two cases (EXP1 and EXP2, respectively), at preselected time intervals for the different grid sizes and the numerical schemes. The shape of the front of the bubble is the same, while the tail

varies but not too significantly, for the different grid sizes and numerical schemes. A distinct interphase was obtained for the very fine mesh (0.61 million cells). Note that one of the preselected time intervals is adopted to correspond to the time interval of the bubble shape captured during the experiment work.

(a) Bubble shape from experiment, EXP1: VOLgas = 0.001498m^3, L_b = 0.2m, Fr = 0.4374

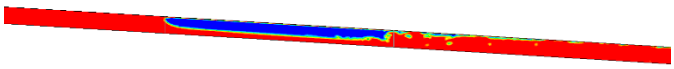

(b) Bubble shape from EXP1_1a, Sim.L_b = 0.89m

(c) Bubble shape from EXP1_2a, Sim.L_b = 0.86m

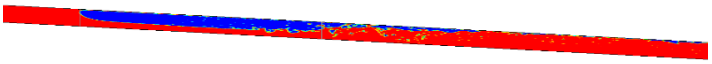

(d) Bubble shape from EXP1_3a, Sim.L_b = 0.90m

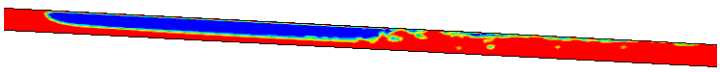

(e) Bubble shape from EXP1_1b, Sim.L_b = 0.89m

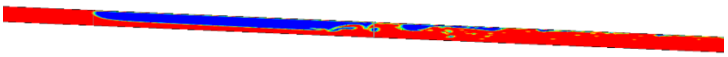

(f) Bubble shape from EXP1_2b, L_b = 0.89m

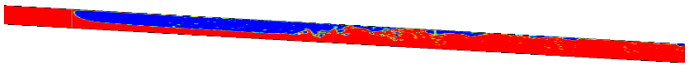

(g) Bubble shape from EXP1_3b, L_b = 0.88m

Figure 3: Bubble shape comparison between simulations and EXP1 (at one of the preselected time intervals for different numerical schemes for 2D model, cf. Table 3)

(a) Bubble shape from experiment, EXP2: VOLgas = 0.002996m^3, L_b = 0.47m, Fr = 0.4394

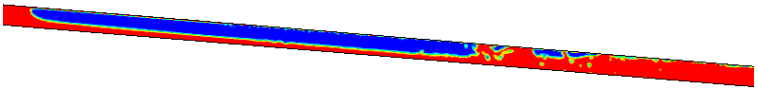

(b) Bubble shape from EXP2_1a, Sim.L_b = 1.975m

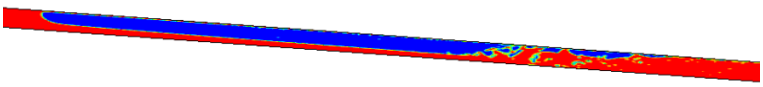

(c) EXP2_2a, Sim.L_b = 1.80m

(d) EXP2_3a, Sim.L_b = 1.90m

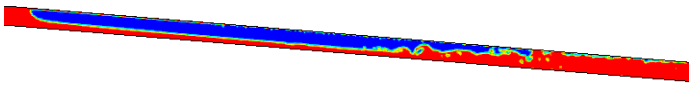

(e) EXP2_1b, Sim.L_b = 02.00m

(f) EXP2_2b, Sim.L_b = 1.99m

(g) EXP2_3b, Sim.L_b = 2.00m

Figure 4: Bubble shape comparison between simulations and EXP2 (at one of the preselected time intervals for different numerical schemes for 2D model, cf. Table 3)

The oil volume fraction distributions established at the 6m-position from the inlet of the 0.099m diameter, 15.7m long pipe at 5° angle of inclination for the different grid sizes and the numerical schemes are presented in Figure 5, for the EXP2 case. The smooth sections of the curves represent the bubbles fronts while the jagged sections depict the bubbles tails. The average area-weighted oil volume fraction around the elongated bubble is about 0.3 for virtually all the different grid sizes and numerical schemes considered. This value is however 42.3% less than the oil volume fraction obtained from the experiment.

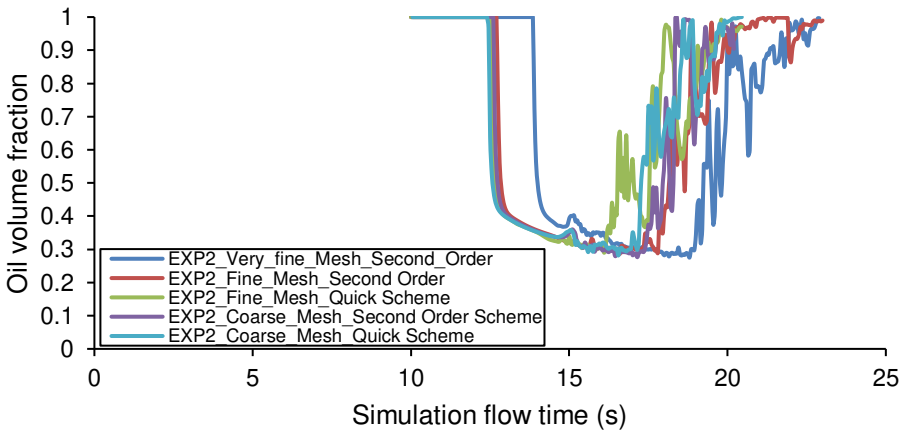

Figure 5: Oil volume fraction distribution at 6m-position for EXP2 CASE

The bubble length is another feature investigated in this work. In the 2D cases presented in Figures 3 and 4, the simulated bubble length is largely over-estimated (about 3-4 times the size of the

experimental one) for the same experimental flow conditions, most especially for low oil viscosity, in this case 160cP. This is due to the simplification of the governing equations of the fluid in a 2D form. This therefore shows a limitation when using a 2D model. Hence, a correction is required to establish the correct values.

3.2 Review of the 2-D inlet (injection) boundary condition

Based on the above observation regarding the bubble length, the 2D inlet (injection) boundary condition was reviewed. The pressure inlet boundary condition was changed to a mass influx inlet boundary condition to ensure that the mass flow rate in a 3D form (which is equivalent to the laboratory condition) is scaled to a 2D form. The results of the bubble length obtained for the simulation case (2D EXP2) show a reduction of about 50% when compared to results obtained with the pressure inlet boundary condition. Though there was an improvement in the bubble length estimation, the result is still overestimated when compared to that of the experimental result. Figure 6 shows the results comparison (of the oil volume fraction 6m far from the inlet) between the pressure inlet boundary condition and the mass flux inlet boundary condition. The offset seen in the plot is due to the velocity at which the gas is injected, different if a Pressure inlet or a Mass flow inlet injection type is applied. For the fixed mass influx boundary condition, the solution shows a bubble velocity lower than when a pressure inlet boundary condition is applied.

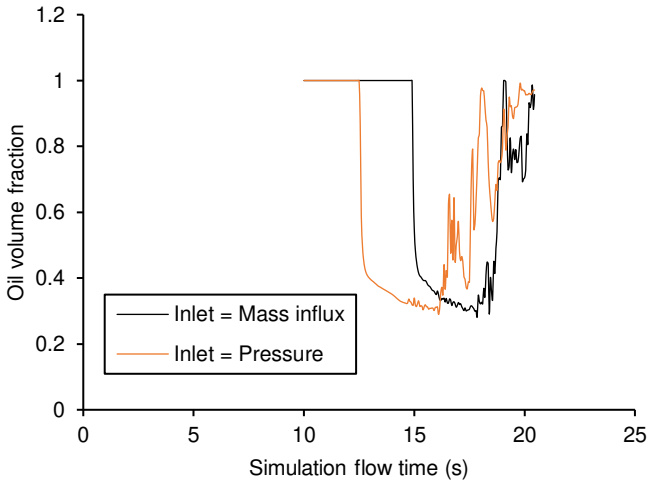

Figure 6: Results comparison between the pressure inlet and mass flux inlet for the simulation case (2D EXP2)

The result of the drift velocity obtained with the mass influx boundary condition is slightly lower than when the pressure inlet boundary condition is used. A discrepancy of 11% is obtained.

3.3 Degeneration of a single elongated bubble with pipe inclination and liquid viscosity

Extended simulations were carried out to investigate the effects of pipe inclination and liquid viscosity on the behavior of a large bubble in stagnant liquid along the pipe. The pipe and fluid conditions for

EXP2 given in Table 2 were used as a base case, with further simulation runs for oil viscosities of 560cP and 1140cP, and pipe inclinations of 7.5°, 10°, 20° and 30°. The liquid density and surface tension for the 160cP viscosity oil were adopted for the 560cP viscosity oil, see Table 4 for the data used for the extended simulation runs. The second order upwind scheme was used for the discretization of the momentum term.

Table 4: Data for the extended simulation runs

Simulation ID	Pipe diam. (m)	Inclination angle (degree)	Inlet pressure (Bar)	Inlet pipe diam. (m)	Injection time (s)	Oil viscosity (cP)	Oil density (Kg/m^3)	Surface tension (N/m)
(Base case 1)	0.099	5	3.8	0.004	2	160	870	0.027
1-1	0.099	7.5	3.8	0.004	2	160	870	0.027
1-2	0.099	10	3.8	0.004	2	160	870	0.027
1-3	0.099	20	3.8	0.004	2	160	870	0.027
1-4	0.099	30	3.8	0.004	2	160	870	0.027
(Base case 2)	0.099	5	3.8	0.004	2	560	870	0.027
2-1	0.099	7.5	3.8	0.004	2	560	870	0.027
2-2	0.099	10	3.8	0.004	2	560	870	0.027
2-3	0.099	20	3.8	0.004	2	560	870	0.027
2-4	0.099	30	3.8	0.004	2	560	870	0.027
(Base case 3)	0.099	5	3.8	0.004	2	1140	960	0.036
3-1	0.099	7.5	3.8	0.004	2	1140	960	0.036
3-2	0.099	10	3.8	0.004	2	1140	960	0.036
3-3	0.099	20	3.8	0.004	2	1140	960	0.036
3-4	0.099	30	3.8	0.004	2	1140	960	0.036

The simulated bubble length of a single bubble was much higher than that of the experimentally observed bubble length for the same flow conditions, especially for the low viscosity oil of 160cP and generally when a pressure inlet boundary condition was used, with pipe inclinations less than 7.5°. A single elongated bubble was seen not to remain constant when the pipe inclination was increased above 7.5°. There was a degeneration of the single bubble into two or more bubbles in the low viscosity oil. Figures 7 to 9 show the plot of the bubble behaviour at the 6m position from the inlet against the pipe

inclination. As can be seen in Figure 7, the single bubble behaviour in a 160cP oil disintegrates into shorter bubbles as the pipe inclination is increased above 5°. This could be due to the increase in the potential energy of the falling liquid, sufficient enough to overcome the cohesive force of the single bubble. However, in medium and high viscous oils, e.g. for 560cP and 1140cP as shown in Figures 8 and 9 respectively, the single bubble remained intact, even when pipe inclination was increased. This observation may therefore imply that under the same flow conditions the slug frequency is expected to be higher in low viscous oils than in medium and high viscous oils when the pipe inclination from horizontal is above 5°. Since the experimental visualization of the bubble was performed at a particular distance (above 6m) from the inlet for pipe inclination under 7.5°, it will be important to obtain experimental data and perform 3D CFD simulations to validate this observation of elongated bubble disintegration in a 2D CFD form as it moves from the point of entrance to the other end of the pipe.

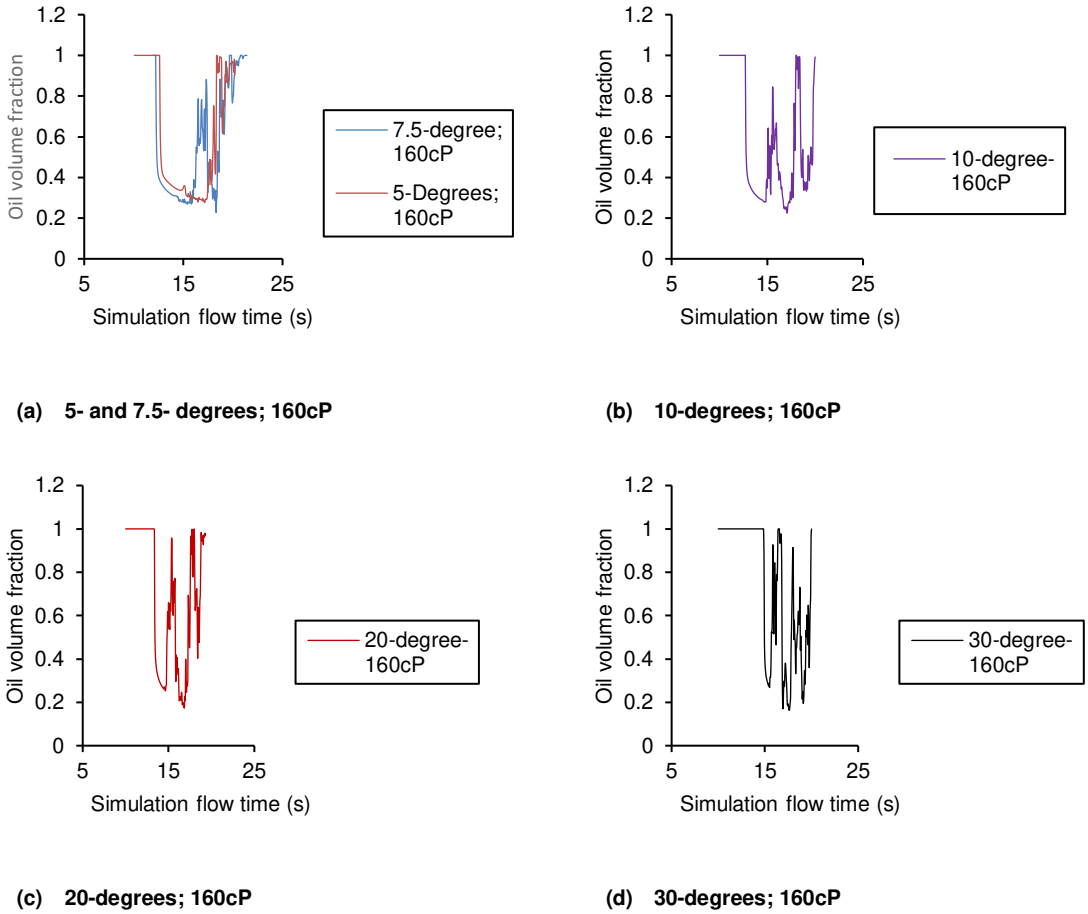

(a) 5- and 7.5- degrees; 160cP

(b) 10-degrees; 160cP

(c) 20-degrees; 160cP

(d) 30-degrees; 160cP

Figure 7: 2D results of the degeneration of single elongated bubble in 160cP liquid in 0.099m ID pipe with inclination

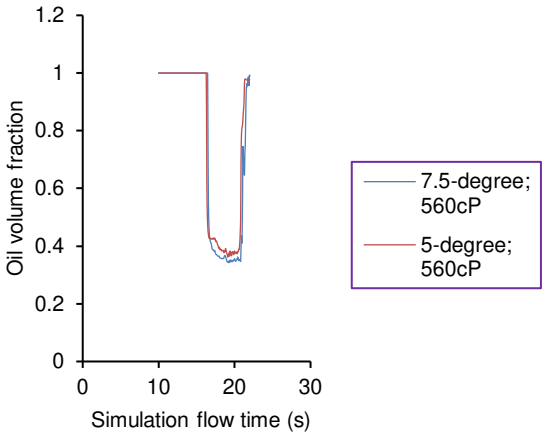

(a) 5- degrees; 560cP

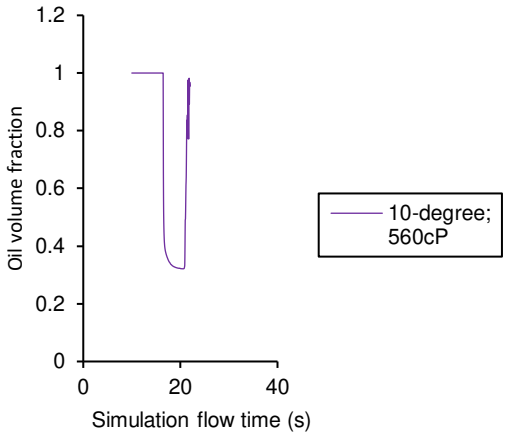

(b) 10-degrees; 560cP

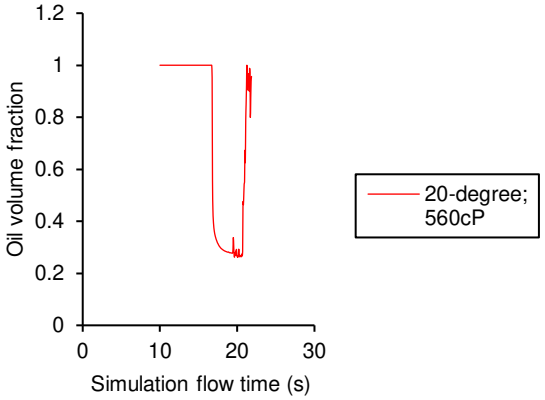

(c) 20-degrees; 560cP

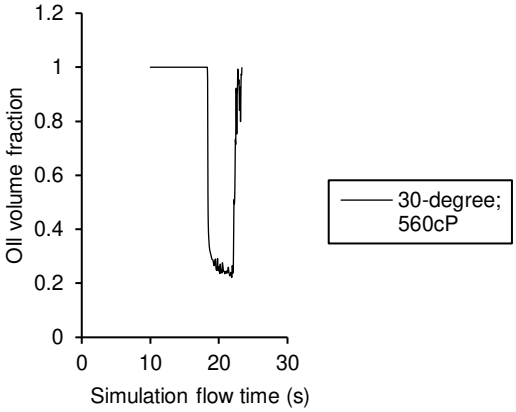

(d) 30-degrees; 560cP

Figure 8: 2D results of the degeneration of single elongated bubble in 560cP liquid in 0.099m ID pipe with inclination

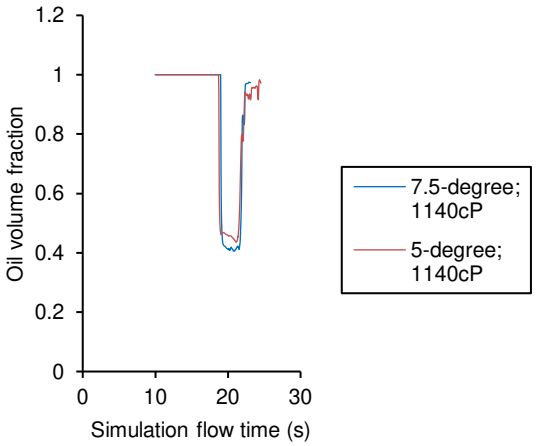

(a) 5- and 7.5- degrees; 1140cP

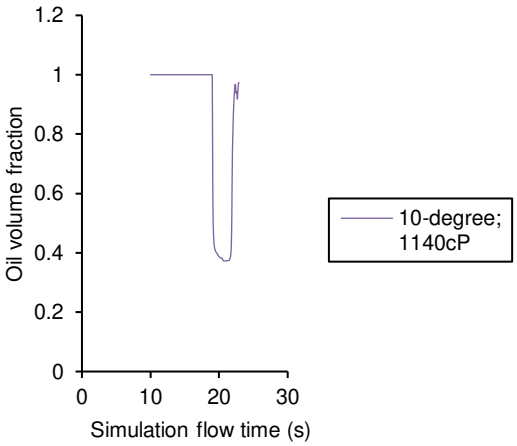

(b) 10-degrees; 1140cP

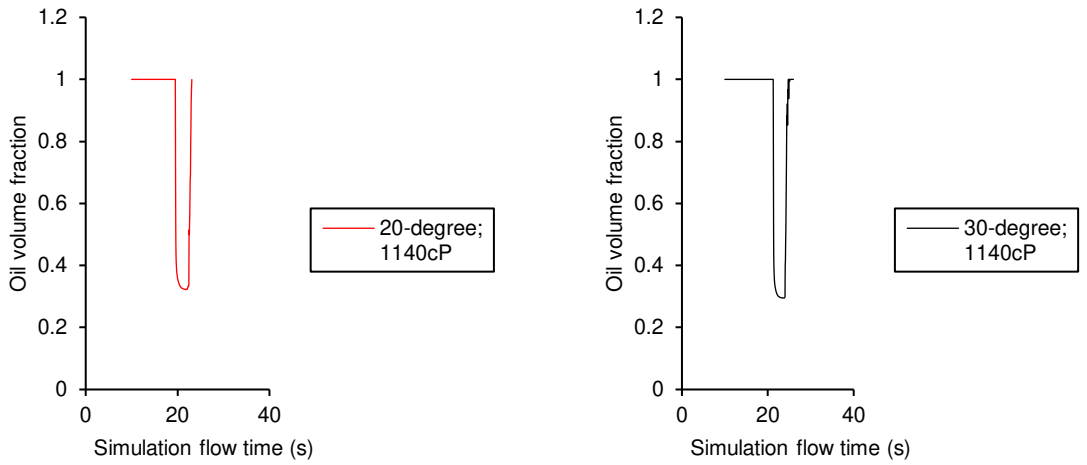

(c) 20-degrees; 1140cP **(d) 30-degrees; 1140cP**

Figure 9: 2D results of the degeneration of single elongated bubble in 1140cP liquid in 0.099m ID pipe with inclination

3.4 2D CFD drift velocity results comparisons with experimental data

The investigation of the effect of pipe inclination and liquid viscosity on the drift velocity of a single elongated bubble in liquid in pipes was carried out. Figure 10 shows the plot of the drift velocity against the pipe inclination. It appears that the drift velocity increases slightly with an increase of pipe inclination but decreases with an increase in liquid viscosity. This is in line with the findings from previous researchers, see for instance, Gokcal et al. [5], Jeyachandra et al. [6], Moreiras et al. [7], Livinus et al. [9], Hua et al. [13], Ben-Mansour et al. [19].

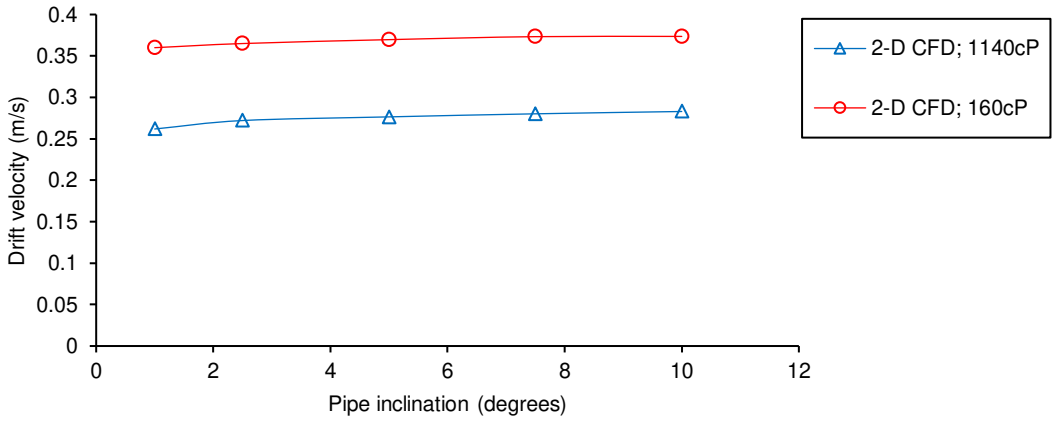

Figure 10: Simulated drift velocity against the pipe inclination

The CFD results were also compared to the experimental results for the same pipe inclination and liquid viscosity of 160cP and 1140cP. The simulated drift velocity results agree fairly with the experimental results, although CFD-based results are under-estimated, see Figure 11.

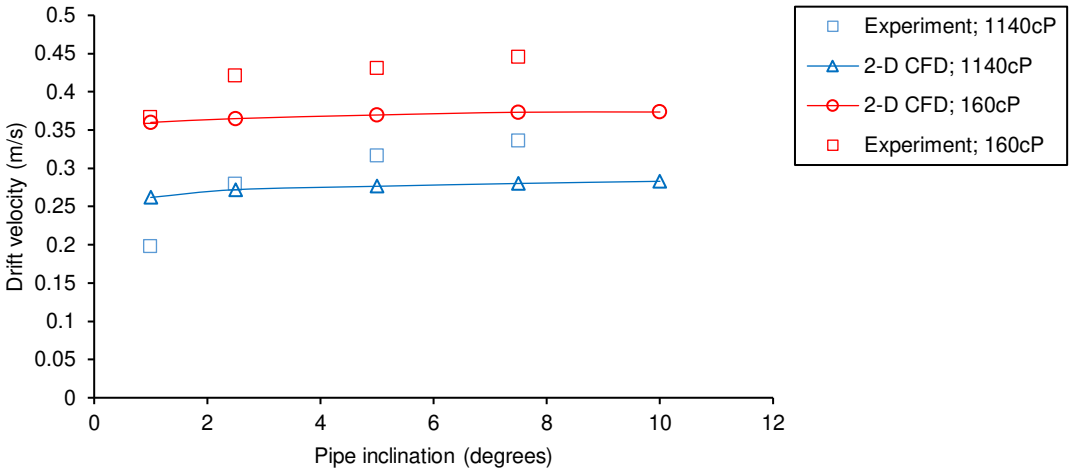

Figure 11: Drift velocity results comparison between experiments and 2D CFD

3.5 2D CFD result for flowing cases

2D CFD simulations were also conducted on a single elongated bubble in a flowing liquid with a range of liquid velocity, 0.102 – 0.32 m/s as applied in the experiments, and for an additional case with liquid velocity of 0.6m/s. Figure 12 shows the variations of the simulated elongated bubble shapes (red colour for liquid, and blue colour for gas) under the effect of the flowing liquid for a 0.102 – 0.6m/s liquid velocity range for a 0.099m diameter pipe with 7.5° to horizontal. Simulated bubble shapes are compared with the corresponding experimental bubble images.

The liquid flows from the bubble tail to the front, pushing the elongated bubble forward along the pipe. The bubble shapes (except the bubble length) at preselected time intervals match fairly the experimental data. As the liquid velocity is increased, the front of the bubble changes from the usual well curved shape inclined towards the top of the pipe wall, to a bubble nose moving away from the pipe wall, and submerging into the liquid inside the pipe, as the bubble advances. Meanwhile, the tail and body changed considerably with time. Entrainment of dispersed gas in the liquid behind the bubble is also observed. Hua et al. [13] attributed the bubble nose moving away from the pipe wall to the presence of high flow resistance due to the high velocity gradients in the liquid between the nose and the pipe wall.

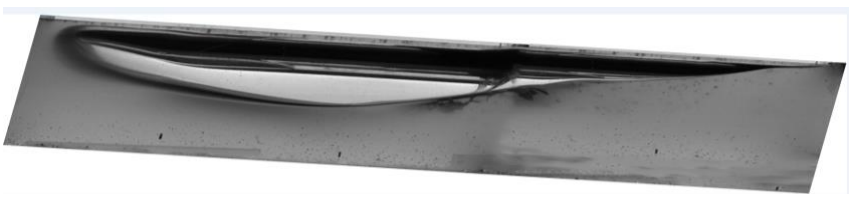

(a) Experimental Bubble shape for EXP3; 160cP oil, Vso = 0.108m/s, VOLgas = 0.001498m^3

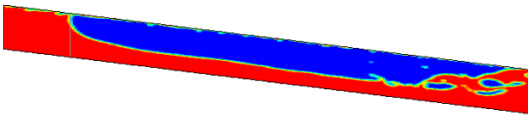

(b) Simulated bubble shape for EXP3, Vso=0.108m/s; @ 3.21m

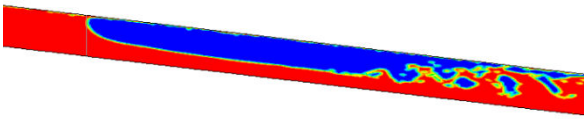

(c) Simulated bubble shape for EXP3, Vso=0.108m/s; @ 3.48m

(d) Experimental Bubble shape for EXP4; 160cP oil, Vso = 0.21m/s, VOLgas = 0.001498m^3

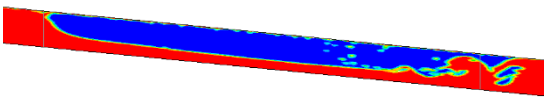

(e) Simulated bubble shape for EXP4, Vso=0.21m/s; @ 6.25m

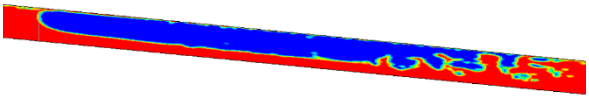

(f) Simulated bubble shape for EXP4, Vso=0.21m/s; @ 6.59m

(g) Experimental Bubble shape for EXP5; 160cP oil, Vso = 0.32m/s, VOLgas = 0.001498m^3

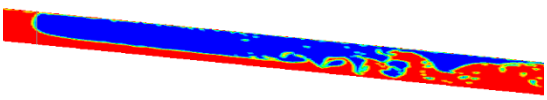

(h) Simulated bubble shape for EXP5, Vso=0.32m/s; @ 5.21m

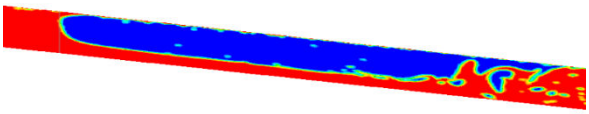

(i) Simulated bubble shape for EXP5, Vso=0.32m/s; @ 7.94m

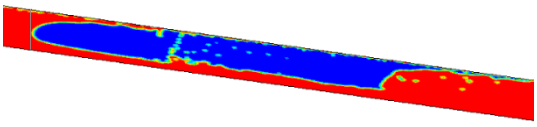

(j) Simulated bubble shape for EXP5, Vso=0.6m/s; @ 5.35m

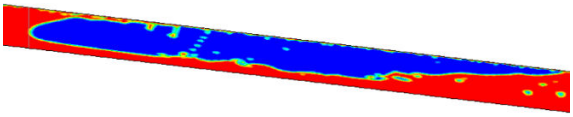

(k) Simulated bubble shape for EXP5, Vso=0.6m/s, @ 6.16m

Figure 12: Various simulated elongated bubble shapes (red colour for liquid, and blue colour for gas) for flowing liquid with 0.102 – 0.6m/s velocity range for a 0.099m diameter pipe with 7.5° relative to horizontal, and the corresponding experimental bubble images.

The propagation speed of elongated bubbles is commonly correlated with the mixture velocity and the bubble drift velocity in flowing liquid by the following correlation:

$$v_t = C_o v_m + v_d \tag{9}$$

where C_o is the velocity distribution coefficient. Hence, a plot of the calculated bubble velocity against the liquid velocity was created, and the drift velocity was obtained by determining the bubble velocity at zero liquid velocity, see Figure 13 for a case at 7.5° inclination to horizontal. The equation on the left hand side of the graph represents the best fit equation. The constant for the equation is the drift velocity of the elongated bubble. As observed from the plot, the bubble velocity varies linearly with the liquid velocity with an R^2-value of 0.98. The velocity distribution coefficient C_o obtained is 0.7528.The estimated drift velocity is thus 0.3242 m/s. The experimental results for this case, the velocity distribution coefficient of 0.9582 and the drift velocity of 0.4439 m/s, compare well with the above calculated values.

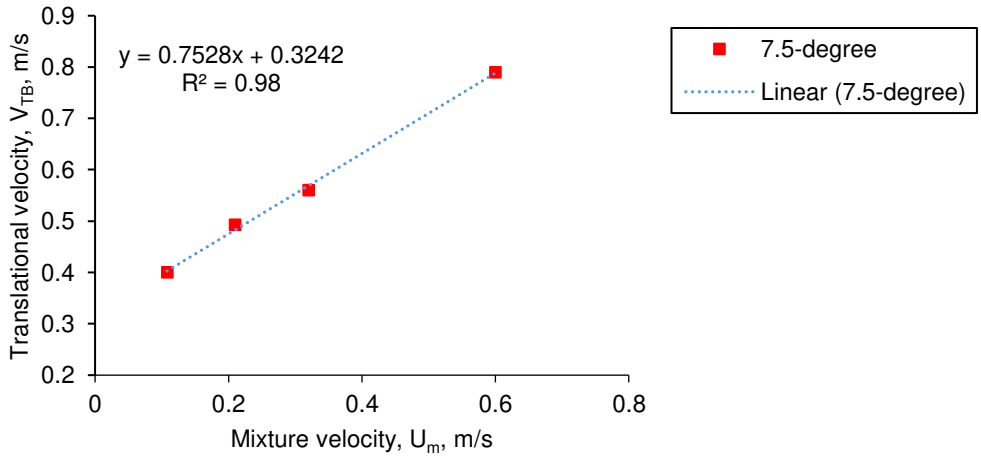

Figure13: Various propagation speeds of the elongated bubble with the mixture velocities in the flowing liquid.

4.0 3D CFD results

Because of the high computational resources involved, it was difficult to perform many 3D simulations. A preliminary numerical calculation has however been done, based on the following experimental data: 160cP oil viscosity, 870kg/m^3 oil density, 1.75kg/m^3 nitrogen gas density, 0.099m pipe diameter, 3.8 bar gas injection pressure. Nitrogen gas was injected for 2 seconds via the 0.004m diameter injection tube, and a 5° pipe inclination was considered. The second order upwind scheme was used for the discretization of the momentum term.

The front of the calculated bubble was well curved and its shape remained constant as the bubble advanced along the pipe. This observation matched the experimental observed bubble shape propagation. However, the entrained tiny bubbles observed both experimentally and in the 2D simulations were not visible for the 3D case.

The calculated drift velocity of the elongated bubble and the gas fraction agreed fairly with the measured data. The simulated drift velocity fluctuated initially as the bubble moved along the pipe but remained constant after the bubble had travelled some distance. There is also a good agreement between the calculated and the measured bubble lengths. Figures 14 to 16 show the bubble shape, drift velocity profile and the estimated bubble length profile, respectively. It appeared that both the drift velocity and the bubble length remained constant after 3-4m, showing some sort of convergence. Both simulated drift velocity and bubble length are however under-predicted when compared to experiments, showing a 16% error for both simulated drift velocity and bubble length. However, those results show a significant improvement over the 2D simulated results.

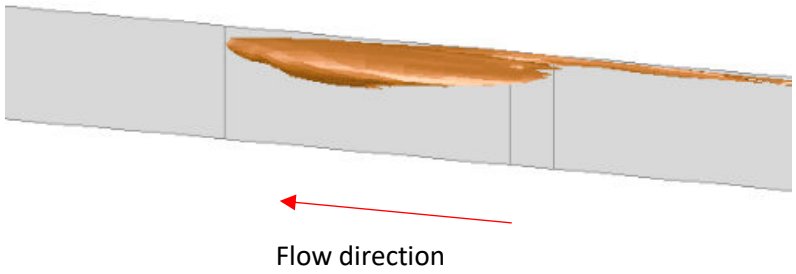

Figure 14: Simulated bubble shape for EXP2; 3D CFD case

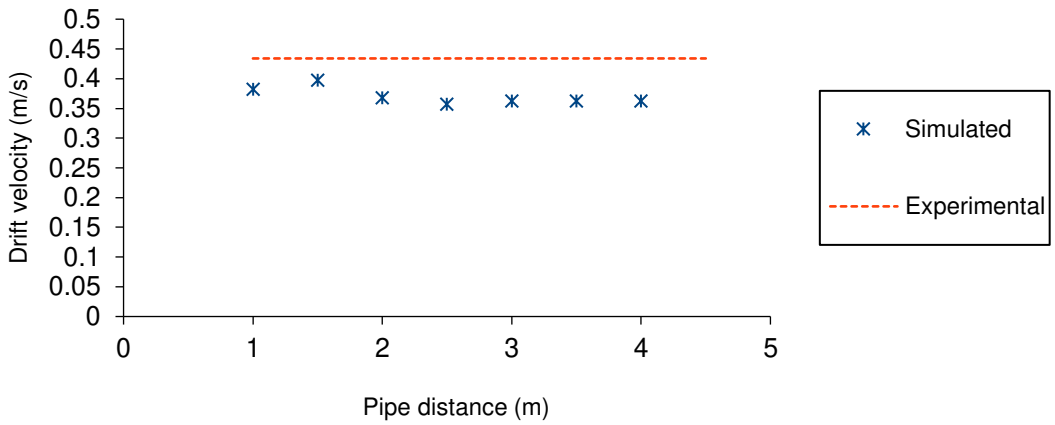

Figure 15: Drift velocity profile for EXP2; 3D CFD case

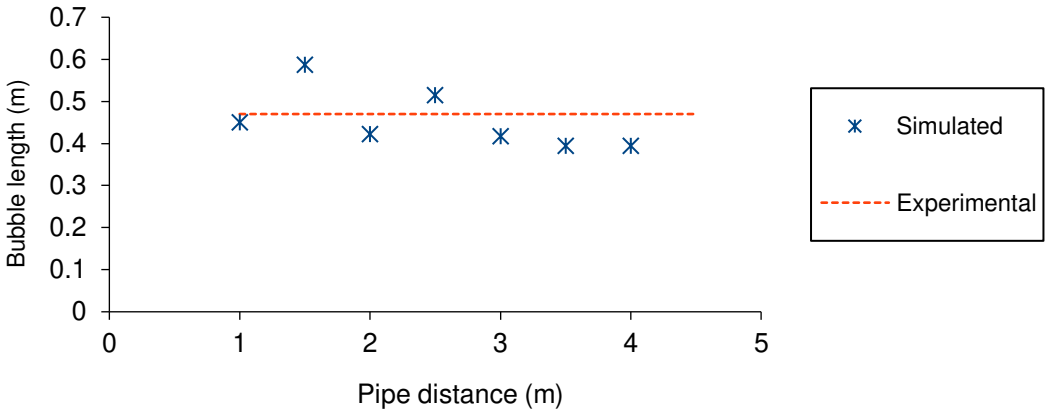

Figure 16: Bubble length profile for EXP2; 3D CFD case

5. Conclusion

Due to the high computational time required for the CFD work, 2D CFD simulations have been preferred to study the effect of pipe inclinations and viscosity on the behaviour of an elongated gas bubble in liquid in pipes. A preliminary 3D numerical calculation has however been conducted. Numerical results have been validated against experimental data, where available. For the 0.099m diameter, 15.7m long pipe at 5° angle of inclination (2D case), at the 6m position, the average area-weighted oil volume fractions around the elongated bubble was about 0.3. This value is 42.3% less than the oil volume fraction obtained in the experiment. The bubble nose shape prediction was however in good agreement while the tail prediction shape agreed fairly with the experimental data. The simulated drift velocity appeared to increase slightly with an increase of pipe inclination but decreased with an increase in liquid viscosity. The simulated 2D and 3D drift velocity results matched the experimental results with an absolute average error of less than 10%. The bubble lengths in the 2D simulations were over-predicted, but there was good agreement between the calculated bubble length and the experimental bubble length for the 3D simulated case.

In the 2D cases, the single elongated bubble was seen not to remain constant when the pipe inclination was increased above 7.5°. There was a degeneration of a single bubble into two or more bubbles in the low viscosity oil. However, in medium and high viscous oils, e.g. the 560cP and 1140cP, the single bubble remained intact, even when the pipe inclination was increased.

The experimental visualization of elongated bubbles reported by Livinus and Verdin [25], and Livinus [26] were performed at a particular distance from the inlet (above 6m), for pipe inclination under 7.5°. It will thus be important in the future to generate experimental data and perform additional 3D CFD simulations to check and validate the elongated bubble disintegration observed in the 2D CFD simulations, as the bubble moves from the point of entrance to the other end of the pipe.

REFERENCES

[1] K.H. Bendiksen, 1984. An Experimental Investigation of the Motion of Long Bubbles in Inclined Tubes. International Journal of Multiphase Flow. 10(4), (1984) 467–483.

[2] M.E. Weber, A. Alarie, and M.E. Ryan, Velocities of extended bubbles in inclined tubes. Chemical Engineering Science. 41(9), (1986) 2235–2240.

[3] A. Hasan, and C. Kabir, Predicting Multiphase Flow Behavior in a Deviated Well, SPE Production Engineering. 3(4) (1988).

[4] Viana et al., 2003. Universal correlation for the rise velocity of long gas bubbles in round pipes. J. Fluid Mech. 494, 379-398. DOI: 10.1017/S0022112003006165.

[5] B. Gokcal, A.S. Al-Sarkhi, and C. Sarica, Effects of high oil viscosity on drift velocity for upward inclined pipes, SPE Annual Technical Conference and Exhibition, ATCE (2008), pp. 963–975.

[6] B.C. Jeyachandra, B. Gokcal, A. Al-Sarkhi, C. Sarica, and A. Sharma, Drift-Velocity Closure Relationships for Slug Two-Phase High-Viscosity Oil Flow in Pipes, SPE Journal (2012).

[7] J. Moreiras, E. Pereyra, C. Sarica, and C.F. Torres, Unified drift velocity closure relationship for large bubbles rising in stagnant viscous fluids in pipes. Journal of Petroleum Science and Engineering. 124, (2014) 359–366.

[8] G. Losi, and P. Poesio, 2016. An experimental investigation on the effect of viscosity on bubbles moving in horizontal and slightly inclined pipes. Experimental Thermal and Fluid Science. 75, (2016) 77–88.

[9] A. Livinus, P. Verdin, L. Lao, J. Nossen, M. Langsholt, H. Sleipnæs, Simplified generalised drift velocity correlation for elongated bubbles in liquid in pipes. Journal of Petroleum Science and Engineering. 160, (2018) 106–118.

[10] M. Cook, and M. Behnia, 2001. Bubble motion during inclined intermittent flow, International Journal of Heat and Fluid Flow. 22(5), (2001) 543–551.

[11] T. Taha, and Z.F. Cui, CFD modelling of slug flow in vertical tubes, Chemical Engineering Science, 61(2), (2006) pp. 676–687.

[12] P.M. Ujang, L. Pan, P.D. Manfield, C.J. Lawrence, F.G. Hewitt, Prediction of the Translational Velocity of Liquid Slug in Gas-Liquid Slug Flow Using Computational Fluid Dynamics, Multiphase Science and Technology, 20(1), (2008) pp. 25–79.

[13] J. Hua, M. Langsholt, C. Lawrence, Numerical simulation of single elongated bubble propagation in inclined pipes, *Progress in Computational Fluid Dynamics, an International Journal*, 12(2/3), (2012) pp. 131–139.

[14] C.W. Hirt, and B.D. Nichols, Volume of Fluid (VOF) Method for the Dynamics of Free Boundaries, J. Comput. Phys. 39. (1981) 201–225.

[15] D.L. Youngs, Time-Dependent Multi-Material Flow with Large Fluid Distortion, Numerical Methods for Fluid Dynamics. K. W. Morton and M. J. Baines, editors. (1982) Academic Press.

[16] S. Osher, and J. A. Sethian, Fronts Propagating with Curvature-dependent Speed: Algorithms Based on Hamilton-Jacobi Formulations. J. Comput. Phys. 79. (1988) 12–49.

[17] P. Andreussi, M. Bonizzi, and A. Vignali, Motion of elongated gas bubbles over a horizontal liquid layer, 14th Int. Conf. Multiph. Prod. Technol., (2009) pp. 309–318.

[18] M. Ramdin, and R. Henkes, Computational Fluid Dynamics Modeling of Benjamin and Taylor Bubbles in Two-Phase Flow in Pipes, ASME J. Fluids Eng. 134(4): (2012) 041303.

[19] R. Ben-Mansour, A. K. Sharma, B. C. Jeyachandra, B. Gokcal, A. Al-sarkhi , C. Sarica, Effect of pipe diameter and high oil viscosity on drift velocity for horizontal pipes, BHR Group - 9th North American Conference on Multiphase Technology, 2-4 June, 2010, Banff, Canada.

[20] A. Liné, R. Belt, J.M. Munoz, O. Allain, and D. Guégan, Data processing of full 3D numerical simulation of slug flow to improve Unit Cell Model, Proceedings of the 16th International Conference on Multiphase Production Technology, (2013), pp. 203–212.

[21] R.F. Kroes, and R.W.M. Henkes, CFD for the motion of elongated gas bubbles in viscous liquid, BHR Group - 9th North American Conference on Multiphase Technology 2014, (1), pp. 283–298.

[22] E. Lizarraga-Garcia, J. Buongiorno, E. Al-Safran, D. Lakehal, 2017. A broadly-applicable unified closure relation for Taylor bubble rise velocity in pipes with stagnant liquid. International Journal of Multiphase Flow. 89, 345–358.

[23] A.M. Deendarlianto, A. Widyaparaga, O. Dinaryanto, Khasani and Indarto, 2016. CFD Studies on the gas-liquid plug two-phase flow in a horizontal pipe, Journal of Petroleum Science and Engineering, 147(2) (2016) pp. 779–787

[24] J. Brackbill, D.B. Kothe, C. Zemach, A continuum method for modeling surface tension. Journal of computational physics, 100(2), (1992) 335-354.

[25] A. Livinus, and P.G. Verdin, Experimental study of a single elongated bubble in liquid in under 10-degree upwardly inclined pipes, Experimental Thermal and Fluid Science (2020), doi: https://doi.org/10.1016/j.expthermflusci.2020.110247

[26] A. Livinus, A study of a single elongated bubble in liquid in pipes, (2018) Ph.D Thesis. Cranfield University, Bedfordshire, UK.

CFD study of the characteristics of a single elongated gas bubble in liquid in a moderately inclined pipe

Livinus, Aniefiok

2021-03-23

Livinus A, Verdin PG. (2021) CFD study of the characteristics of a single elongated gas bubble in liquid in a moderately inclined pipe. Upstream Oil and Gas Technology, Volume 7, September 2021, Article number 100037

https://doi.org/10.1016/j.upstre.2021.100037